Netherlands Journal of Geosciences — Geologie en Mijnbouw | 91 – 3 | 357 - 372 | 2012

Towards a process-based model to predict dune erosion along the Dutch Wadden coast

B.G. Ruessink[1,*], M. Boers[2], P.F.C. van Geer[2], A.T.M. de Bakker[1], A. Pieterse[1], F. Grasso[1] & R.C. de Winter[1]

1 Department of Physical Geography, Institute for Marine and Atmospheric Research Utrecht, Faculty of Geosciences, Utrecht University, P.O. Box 80115, NL-3508 TC Utrecht, the Netherlands.

2 Deltares, P.O. Box 177, NL-2600 MH Delft, the Netherlands.

* Corresponding author. Email: b.g.ruessink@uu.nl.

Manuscript received: May 2011, accepted: December 2012

Abstract

An equilibrium dune-erosion model is used every six years to assess the capability of the most seaward dune row on the Dutch Wadden islands to withstand a storm with a 1 in 10,000 probability for a given year. The present-day model is the culmination of numerous laboratory experiments with an initial cross-shore profile based on the central Netherlands coast. Large parts of the dune coast of the Wadden islands have substantially different dune and cross-shore profile characteristics than found along this central coast, related to the presence of tidal channels, ebb-tidal deltas, beach-plains and strong coastal curvature. This complicated coastal setting implies that the predictions of the dune-erosion model are sometimes doubtful; accordingly, a shift towards a process-based dune-erosion model has been proposed. A number of research findings based on recent laboratory and field studies highlight only few of the many challenges that need to be faced in order to develop and test such a model. Observations of turbulence beneath breaking waves indicate the need to include breaking-wave effects in sand transport equations, while current knowledge of infragravity waves, one of the main sand transporting mechanisms during severe storm conditions, is strongly challenged by laboratory and field observations on gently sloping beaches that are so typical of the Wadden islands. We argue that in-situ and remote-sensing field observations, laboratory experiments and numerical models need to be the pillars of Earth Scientific research in the Wadden Sea area to construct a meaningful process-based dune-erosion tool.

Keywords: dunes; dune erosion; storm waves; equilibrium model; beach-plain; field measurements; laboratory experiments

Introduction

For many coasts wind-blown dunes form the last line of natural defense against high waves and water levels during storms. The assessment whether dunes are sufficiently safe to withstand a storm with a particular frequency of occurrence is top priority for coastal communities where the overtopping or breaching of dunes would result in serious coastal flooding and in the associated loss of life and property. Reliable methods to predict the impact of a storm on a dune, for example, in terms of erosion volume, post-storm erosion profile, or recession distance, are thus of utmost importance. Current methods range from simple empirical equilibrium rules (e.g., Van de Graaff, 1977; Vellinga, 1983, 1986), through analytical wave-impact models (e.g., Overton et al., 1994; Larson et al., 2004) to complicated process-based numerical models that aim to explicitly describe the interaction between the water motion (turbulence, waves, mean flows), sand suspension and transport, and the eroding dune (e.g., Roelvink et al., 2009). The main advantage of an equilibrium or a wave-impact model is its simplicity: it is easy to apply, it requires only a few, often simplified input parameters and it can be set realistically in a probabilistic setting to relate dune erosion to frequency of occurrence. Its simplicity is also its main drawback. Typically, an equilibrium or wave-impact

https://doi.org/10.1017/S0016774600000494 Published online by Cambridge University Press

model is a local model that describes the evolution of a single, often idealised cross-shore profile. Yet, observations have indicated that coastal erosion is often surprisingly variable on a regional scale (e.g., McNinch, 2004; Schupp et al., 2006), related to offshore variable morphology such as outcrops, channels or ebb-tidal deltas. To handle such complicated coastal settings, a regional-scale process-based approach may be more appropriate (e.g., Roelvink et al., 2009; McCall et al., 2010).

The breaking of the incident storm waves lies at the core of the many interacting hydrodynamical and sediment transport processes that ultimately result in dune erosion. From a fluid-mechanics point-of-view, this breaking implies a complete transformation of the organised wind-generated waves into motions at both smaller and larger scales. The small-scale motions comprise breaking-induced turbulence that is likely to be the primary mechanism to suspend sand from the eroding beach into the water column (e.g., Nadaoka et al., 1988). The large-scale motions include 20-200 s waves – infragravity waves – that are related to the grouped structure of the incident wind waves, and mean flows, such as the cross-shore undertow. Both large-scale motions are assumed to be crucial to the seaward transport of the suspended sediments (e.g., Russell, 1993; Van Thiel de Vries et al., 2008). The nature of wave attack on the dunes can be in the form of wave run-up, when incident breaking waves (bores) and infragravity waves hit the base of the dune, or in the form of direct impact on the dune face. Both modes of wave attack lead to dune failure by means of various types of mass movement, including avalanching, overturning, sliding and rotational slumping (e.g., Carter and Stone, 1989; Nishi and Kraus, 1996). Yet, we are just beginning to see the full complexity of breaking waves, turbulence, infragravity waves, mean flows, sand suspension and transport, and the eroding beach and dune. Consequently, process-based storm-impact models are at their infancy and not yet ready to be embedded in the practical assessment of dune safety.

The Netherlands form a prime example where the assessment of dune safety is thoroughly embedded in coastal-zone-management policy. Approximately 70% of the approximately 350-km long Dutch coast consists of high, yet narrow dunes that protect vast, low-lying, densely populated areas against coastal flooding. The existing standards for coastal flood protection date back to the 1970s and were motivated by the 1953 storm surge disaster. A dune is considered to be safe when it will not breach during a storm with an occurrence probability of 1 in 10,000 for a given year. The Netherlands are also a prime example where simple and complicated dune-erosion models must work in concert. On the one hand, the approximately 120-km long central Holland coast is a relatively uniform coast (e.g., Short, 1992) for which an equilibrium model is nowadays applied to assess dune safety (e.g., TAW, 1995; ENW, 2006). On the other hand, the Delta area in the southwestern part of the Netherlands and the Wadden islands in the north (Fig. 1) have

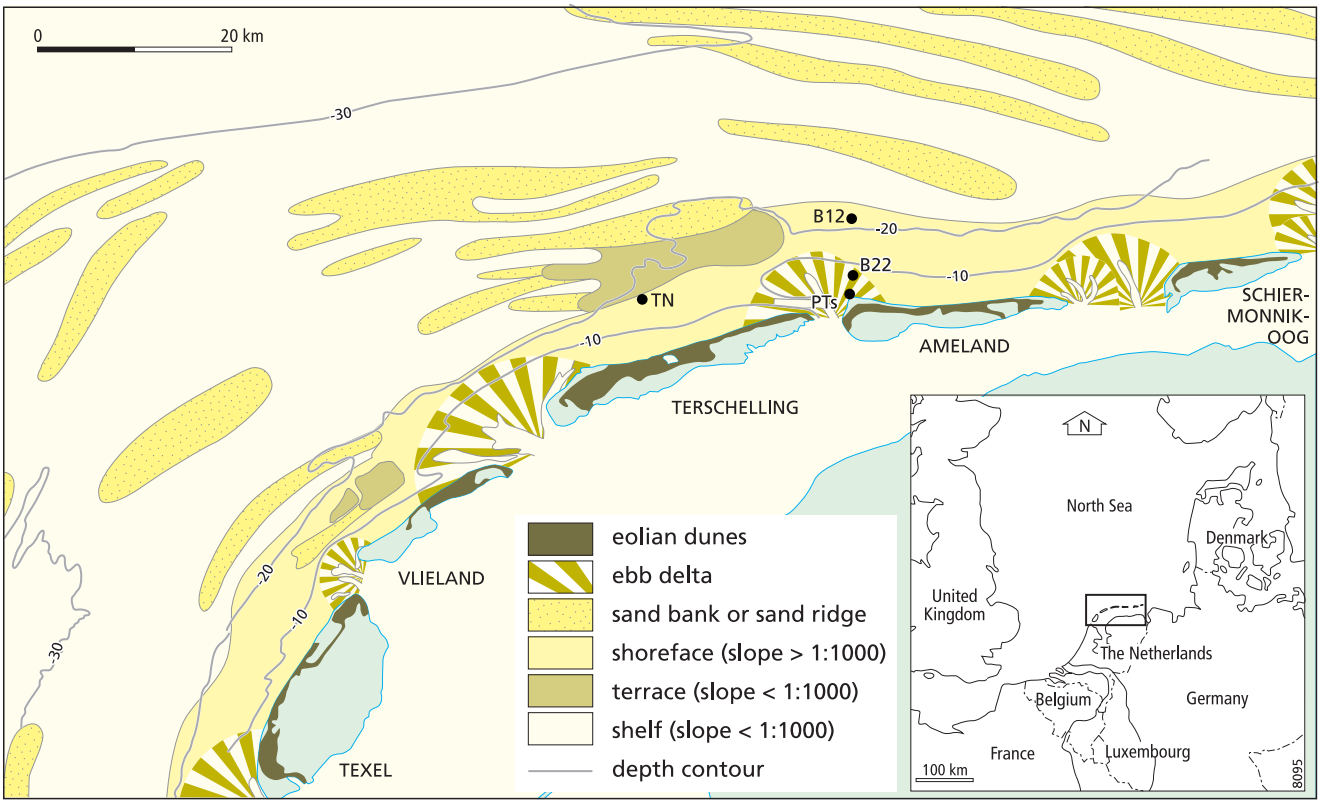

Fig. 1. Geomorphological map of the barrier island coast in the northern part of the Netherlands (adapted from Van Alphen and Damoiseaux, 1987). The dots labeled TN, B12, B22 and PTs are locations of instruments referred to in the Field Studies section of this paper.

https://doi.org/10.1017/S0016774600000494 Published online by Cambridge University Press

a complicated coastal setting with tidal channels and ebb-tidal deltas, spatially extensive beach-plains, and strongly curved coastlines. The aim of this paper, as part of the theme 'Earth Scientific Research in the Wadden Sea Area', is to provide insight into how the complicated coastal setting of the Wadden islands affects the applicability of the current Dutch dune-erosion assessment tool and to highlight a number of research findings that are meant to support a shift from an equilibrium to a process-based assessment tool.

This article is structured as follows. We start off with a non-exhaustive, historical overview of the Dutch dune-erosion assessment methodology, from the Provisional Guideline adopted in the 1970s to the DUROS+ concept applied since 2006. Then we provide glimpses of results of laboratory and field measurements that were specifically designed with some of the unique characteristics of the Wadden-island beaches in mind: their very low slope in the intertidal area (typically, 1:80, as opposed to 1:20-1:30 along the Holland coast) and the up to 500-m wide supratidal beach-plain that in some places separates the dunes from the intertidal beach. The final section summarises the paper.

Dune-erosion policy

Provisional Guideline

The first Dutch tool to assess the capability of dunes to withstand a severe storm was constructed in the early seventies based on dune-beach profile observations collected along the central Dutch Holland coast in the aftermath of the 1953 storm-surge disaster (Van de Graaff, 1977; Vellinga, 1982). The 1953 surge caused the dune front to recede by 10 to 20 m (e.g., Ruessink and Jeuken, 2002), corresponding to a dune erosion quantity of some 60 to 150 m^3/m. The observations resulted in the concept that the erosion profile seaward of the new steep (typically, 1:1) dune front was of constant (i.e., equilibrium) form and could be approximated by a simple relationship:

$$z = 0.415(x + 4.5)^{0.5} - 0.88 \quad (1)$$

where z is the depth below the maximum water level during the storm surge and x is the distance from the intersection of the beach profile and the maximum water level (Fig. 2a), positive in the seaward direction. This profile is applicable from the post-storm dune front (x = 0 m, z = 0 m) up to a water depth below the storm-surge level that was set to 1.28 $H_{s\ br}$, where $H_{s\ br}$ is the significant breaker height. By assuming that the equilibrium profile given by Eq. (1) is also present after the 1:10,000 storm-surge and by applying a cross-shore mass balance, it is possible to reconstruct the cross-shore profile after the design storm-surge. From this profile, the total dune erosion and dune-crest recession distance can be computed.

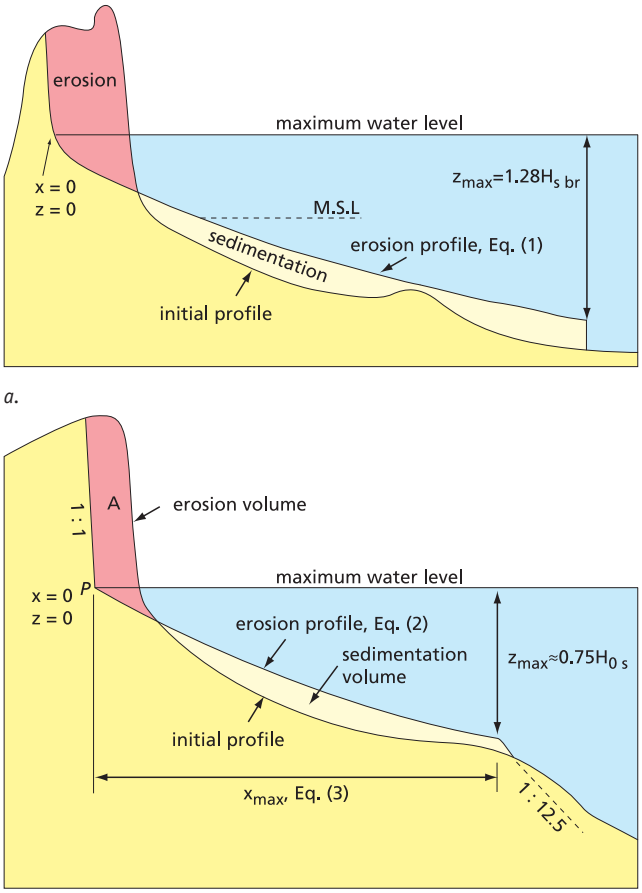

Fig. 2. Schematic diagram of a. the Provisional Guideline; and b. DUROS (after Vellinga, 1982 and ENW, 2006, respectively).

DUROS

Because the first tool was provisional, it was decided to further investigate dune erosion during design conditions by means of physical (laboratory) experiments. Although a process-based model approach was recognised to be potentially more meaningful, it was considered to be impracticable because of a lack of fundamental knowledge on the water motion, sand suspension and sand transport during severe breaking-wave conditions (Van de Graaff, 1977). Results of the laboratory tests can be found in Van de Graaff (1977) and Vellinga (1982, 1983). The initial coastal profile in prototype, termed the reference profile, is provided in Fig. 3. It is highly schematised, comprising a gently sloping profile (1 : 180 to 1 : 20) with a steep (1 : 3) dune with its crest level at 15 m above mean sea level (MSL). The reference profile was considered to be representative of the Holland coast. The laboratory experiments were carried out as two-dimensional tests, implying that dune erosion is assumed to be a two-dimensional problem with offshore-directed sand transport. In a series of tests in a 30 × 30 m wave basin, Vellinga (1982) found no noteworthy alongshore variations in dune erosion and concluded that two-dimensional tests were fully acceptable. In the design and analysis of the laboratory

https://doi.org/10.1017/S0016774600000494 Published online by Cambridge University Press

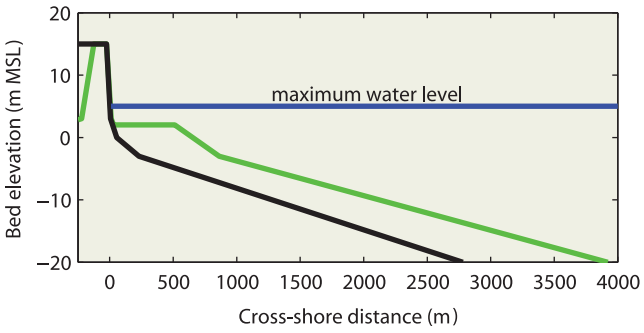

Fig. 3. Reference profile (black) in prototype used in the laboratory experiments that resulted in DUROS and DUROS+. The green line is a modified reference profile used in the Laboratory Experiments section of this paper to examine the effect of a beach-plain (here, 400 m wide and at 2 m +MSL) on dune erosion volumes.

tests, considerable effort was devoted to construct scaling laws to appropriately relate dune erosion volumes in small- and large-scale laboratory settings to prototype. A recent overview of the scaling laws for dune erosion processes can be found in Van Rijn et al. (2011) and is not reiterated here.

The laboratory tests that resulted in the scaling laws were based on time-invariant wave- and surge-conditions. Based on a large-scale test with a realistic North-Sea hydrograph with a peak at 5 m +MSL (Fig. 4b), Vellinga (1986) observed that the cumulative erosion with time-varying conditions was reached after approximately 5 hours (in prototype) with time-invariant, maximum wave and waterlevel conditions (offshore significant wave height H_{0s} of 7.6 m and a water level of 5 m +MSL), see Fig. 4a. Ultimately, the small- and large-scale tests with time-invariant conditions resulted in a new guideline, called DUROS, in which Eq. (1) was replaced by (Vellinga, 1983, 1986; see Fig. 2b)

$$\left(\frac{7.6}{H_{0s}}\right) z = 0.47 \left[\left(\frac{7.6}{H_{0s}}\right)^{1.28} \left(\frac{w}{0.0268}\right)^{0.56} x + 18\right]^{0.5} - 2.00 \quad (2)$$

Here, w is the sediment fall velocity. 'Offshore' is taken as the location with a bed elevation of 20 m below MSL. The erosion profile stretches from the new dune foot (x = 0 m, z = 0 m) to a transition point at a distance of

$$x_{max} = 250 \left(\frac{H_{0s}}{7.6}\right)^{1.28} \left(\frac{0.0268}{w}\right)^{0.56} \quad (3)$$

This implies that the erosion profile ends at $z_{max} \approx 0.75\ H_{0s}$, substantially less than in the Provisional Guideline. For H_{0s} = 7.6 m, w = 0.0268 m/s (median grain size d_{50} = 225 µm) and a water level of 5 m +MSL, the eroded sand thus remains within 250 m from the new dune face at elevations above the 'normal' low-tide line. At the seaward side, the erosion profile is connected to the initial profile with a slope of 1 : 12.5, while a 1 : 1 dune front is assumed above z = 0 m (Fig. 2b). The near-vertical front is consistent with field observations during and immediately after dune erosion (e.g., Carter and Stone, 1989). As with the Provisional Guideline, the amount of erosion follows from a cross-shore mass balance of erosion and sedimentation. As is obvious from Fig. 2b, the erosion profile is less steep than the initial profile. The general lowering of the beach slope as a storm is progressing will cause more profound wave breaking seaward of the dune and, accordingly, lessen the rate of dune erosion with time. This is confirmed by the laboratory experiments (Fig. 4a, blue line).

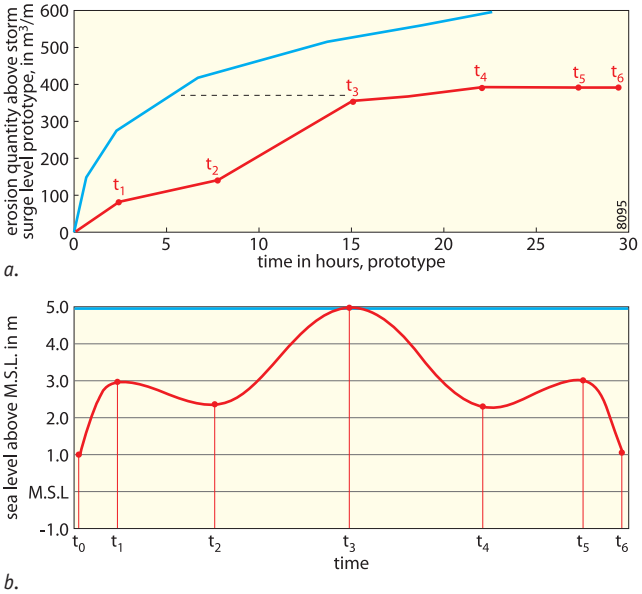

Fig. 4. a. Temporal evolution of the erosion volume above storm surge level during a small-scale laboratory test with (in blue) constant water level and (in red) time-varying water level. Panel (b) shows both water level series. The dashed black line in (a) indicates that the erosion volume in the test with time-varying water levels is reached after about 5 hours with constant maximum water level (after Vellinga, 1986).

DUROS signifies that the amount of dune erosion depends on the hydraulic load on the dunes (significant offshore wave height and the maximum surge level) and on dune strength (sediment characteristics and, by means of the cross-shore mass balance, the initial bed profile). Van de Graaff (1986) argued that the amount of erosion will additionally depend on the storm surge duration and the occurrence of short-period variations in surge levels related to, for example, the passage of showers or fronts. Uncertainties in all these factors will cause the estimated amount of erosion to differ from the 'true' amount of erosion. To this end, the computational method was embedded in a probabilistic setting (Van de Graaff, 1986). This relates the recession distance to a frequency of occurrence. Also, various ad-hoc solutions were implemented to deal with strongly curved coasts, where clearly the assumption of two-dimensionality does not hold and eroded sand is likely to be lost alongshore. The DUROS methodology replaced the Provisional Guideline in 1984. A full description of the computational method can be found in TAW (1995).

https://doi.org/10.1017/S0016774600000494 Published online by Cambridge University Press

DUROS+

The DUROS method is based on a storm peak-wave period T_p of 12 s and does not contain a T_p dependence. This was based on a series of laboratory tests with different offshore wave steepness (0.02-0.04) but no discernable difference in erosion volume (Vellinga, 1983, 1986). Analysis of long-term wave data indicated that T_p varies along the Dutch coast and can also be considerably larger than 12 s. Despite Vellinga's (1983, 1986) observations, it was feared that a larger wave period would increase the amount of dune erosion substantially (Steetzel, 2002). Accordingly, new two-dimensional, small-scale (Coeveld et al., 2005) and large-scale (Van Gent et al., 2008) laboratory experiments were carried out to quantify the effect of T_p on dune erosion and, if necessary, to modify the DUROS method. Furthermore, extensive process measurements were conducted during the large-scale tests (see Van Thiel de Vries et al., 2008) to facilitate the development and testing of a process-based dune-erosion model. The tests indicated that an increase in T_p from 12 to 18 s increased the dune erosion volume by some 20%, substantially less than initially feared (Deltares, 2007). Van Gent et al. (2008) modified DUROS into DUROS+,

$$\left(\frac{7.6}{H_{0s}}\right) z = 0.47\left[\left(\frac{7.6}{H_{0s}}\right)^{1.28}\left(\frac{12}{T_p}\right)^{0.45}\left(\frac{w}{0.0268}\right)^{0.56} x + 18\right]^{0.5} - 2.00 \quad (4)$$

The cross-shore location where the erosion profile changes into the 1:12.5 slope, x_{max}, remained as given by Eq. (3), but z_{max} now is

$$z_{max} = \left(\frac{H_{0s}}{7.6}\right)\left[0.4714\left(250\left(\frac{12}{T_p}\right)^{0.45} + 18\right)^{0.5} - 2\right] \quad (5)$$

This implies that the length of the erosion profile is independent of the wave period but that the value of z_{max} decreases with the wave period. Eqs (4) and (5) can be applied for the range $12 < T_p < 20$ s. When T_p is less than 12 s, $T_p = 12$ s has to be used. When T_p exceeds 20 s, T_p is set to 20 s. DUROS+ replaced DUROS in Dutch coastal policy in 2006. A full description can be found in ENW (2006).

Flood risk maps

DUROS+ is a deterministic, cross-shore dune-erosion model that predicts the post-storm equilibrium profile given schematised hydraulics load (H_{0s}, T_p and maximum waterlevel) and dune characteristics (sediment fall velocity and initial profile). From the shape of the equilibrium profile and a cross-shore balance between erosion and sedimentation, the actual erosion profile can be computed, as well as the dune recession distance. If the dune top in the erosion profile is above the maximum water level, the dune does not breach and is thus sufficiently wide to prevent the hinterland from flooding. The probabilistic model, originally due to Van de Graaff (1986), relates recession distance to a frequency of probability. Within the Dutch coastal policy, a dune is safe when it does not breach with an occurrence probability of 1 in 10,000 for a given year. With DUROS+ and the probabilistic model it is also possible to predict for which occurrence probability a dune will breach. When such a prediction is coupled to a digital elevation model (e.g., in a GIS), it becomes possible to make flood risk maps (Boers et al., 2011). Figure 5 shows such a map for the central part of Ameland; the recession lines in this map are constructed by alongshore connecting the new dune top in each cross-shore profile. In the Ameland map, parts of the dunes are predicted to breach with an occurrence probability between 1:20,000 and 1:40,000. The area that will then flood is indicated with the blue colour and can be used to inform local stakeholders about the risk of having property or infrastructure near the sea.

Further developments

Despite the various modifications from the Provisional Guideline into DUROS+, the actual application of DUROS+ to large parts of the dune coast of the Wadden islands is doubtful. The main reason is that these parts have substantially different dune and cross-shore profile characteristics than found along the Holland coast, on which (by means of the reference profile, Fig. 3) DUROS+ and its predecessors have been based. The main differences are (see also Diermanse et al., 2011):

- Large parts of the heads of Wadden islands are sheltered by ebb tidal deltas (Fig. 1) that are located between the –20 m MSL location and the nearshore. The deltas will dissipate part of the energy of the incident storm waves. In such a case, the –20 m MSL wave conditions will overestimate the wave conditions closer to the beach. As a consequence, the dune erosion volume will be overestimated and, potentially, the dunes are incorrectly considered to be unsafe. Walstra et al. (2008), Huisman et al. (2010) and Diermanse et al. (2011) have proposed a methodology whereby the shape of the erosion profile remains unaltered (i.e., DUROS+) and the wave input is adjusted for energy loss over a shallow area. This methodology, termed D++ (Huisman et al., 2010), has at the moment of writing not yet replaced DUROS+ as the official dune erosion assessment tool. Computations reported in Diermanse et al. (2011) indicate that the reduction in recession distance can increase to over 50% near the heads of the Wadden islands.
- The first dune row in some transects is quite narrow and is likely to breach during conditions that may recur more often than with a 1 in 10,000 probability. For example, a flood risk map for the northwestern part of Vlieland (Boers et al., 2011) shows that some dunes may already breach with a probability of 1 in 100 to 500 years. If and how the erosion of the second dune row has to be considered, is strongly debated.
- The deep tidal channels near the heads of the Wadden islands confuse the mass balance concept when the 1:12.5 part of the erosion profile extends into the channel. The unrealistic

https://doi.org/10.1017/S0016774600000494 Published online by Cambridge University Press

infilling of the channel implies an over-estimation of the amount of deposited material and, hence, of the erosion volume.

– The heads of the islands are strongly curved, at several locations more than 24° per alongshore kilometre. This has two main effects. Firstly, the shoreline curvature will result in gradients in alongshore sand transport. These gradients are negative, in other words, part of the eroded volume will be lost alongshore rather than be deposited within the eroding profile. This causes the rate in dune erosion to remain

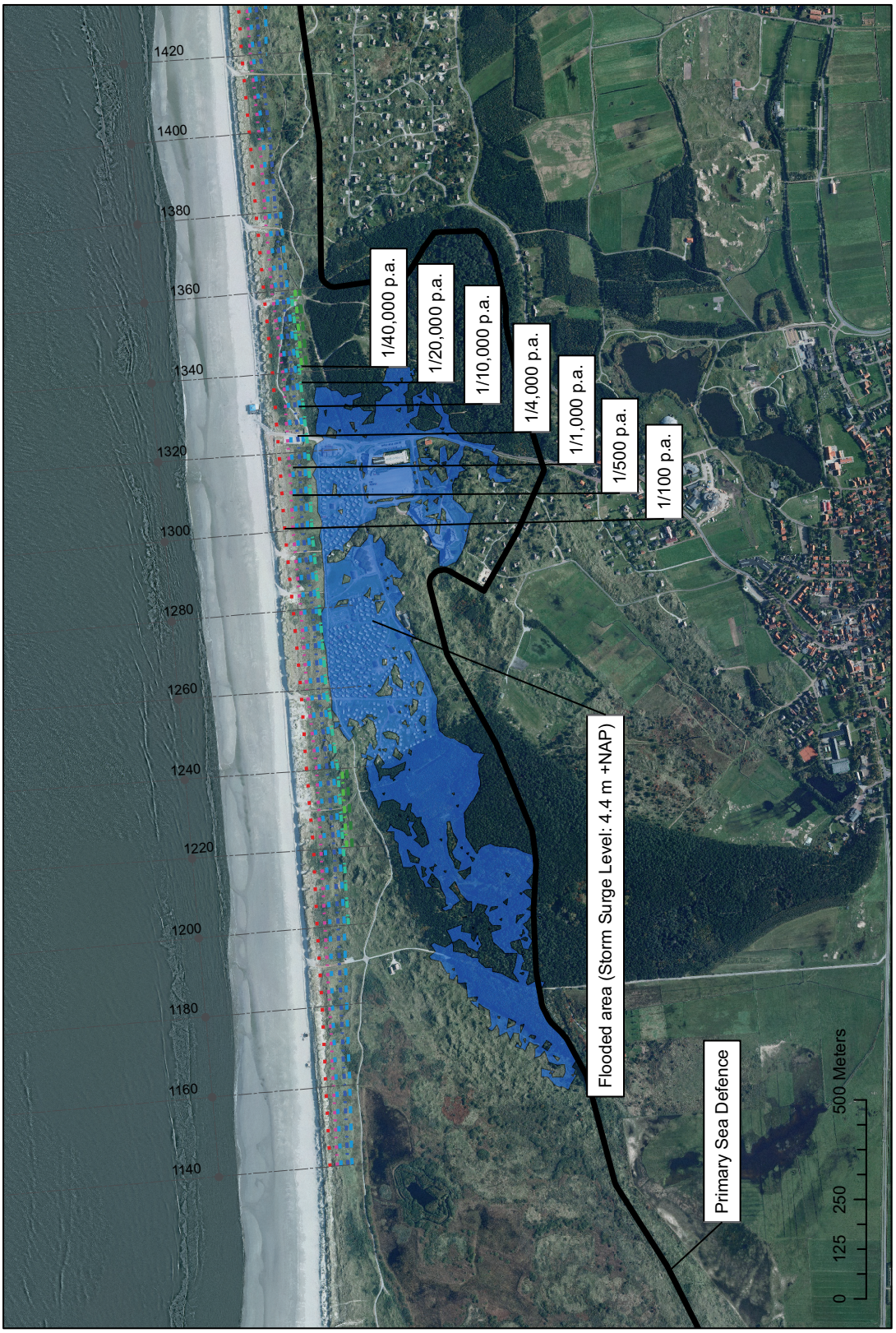

Fig. 5. Flood risk map for the central part of Ameland. The dashed lines are recession lines for the indicated occurrence probability. For an occurrence probability between 1 : 20,000 and 40,000 the dunes between alongshore distance 1240 and 1340 are predicted to breach. The hinterland that is then flooded is indicated with the blue color. After Boers et al. (2011).

https://doi.org/10.1017/S0016774600000494 Published online by Cambridge University Press

higher than in a pure alongshore-uniform case, leading to an overall larger erosion volume. For coasts curving more than 6° per alongshore kilometre this increased loss is embedded within the cross-shore mass balance by simply increasing the erosion volume (e.g., ENW, 2006). For situations with a curvature of more than 24° per alongshore kilometre, ENW (2006) does not state the expected magnitude of the additional loss; instead, it is mentioned that further research is necessary. Secondly, the strong curvature causes part of the dune coast to face the Wadden Sea rather than the North Sea. Wave computations indicate that here the peak wave period can be less than 12 s (Diermanse et al., 2011), falling outside the range on which DUROS+ is based. As aforementioned, the peak wave period has to be raised to be 12 s and, as a result, the dune erosion volume for the parts of the coast facing the Wadden Sea is likely to be too high.

– The slope of the initial profile is often substantially less than that of the erosion profile, i.e., Eq. (4). This is fundamentally different from DUROS+, in which the initial profile is supposed to be steeper than the erosion profile (e.g., Fig. 2b). Because of the very gentle slope, the point (x_{max}, z_{max}) lies below rather than above the initial profile; in other words, the erosion profile does not fit. The gently slopes are particularly present near the heads of the islands, where extensive, virtually flat beach-plains (backshore) are present between the intertidal beach and the first dune row (e.g., Fig. 6). It is expected that the beach-plain reduces the incoming waves during storm-surge conditions such that dune erosion is essentially minimal.

These five differences imply that the dune safety cannot be judged correctly with DUROS+. D++ is a potential candidate to handle the first difference. Because further modifications to DUROS+ and D++ are not considered feasible, a shift towards a process-based dune-erosion model has been proposed. Predictions from this model are thus to replace the entirely empirical Eq. (4). Walstra et al. (2008) compared various process-based models, including DUROSTA (Steetzel, 1993), SBeach (Larson and Kraus, 1989) and XBeach (Roelvink et al., 2009), with a focus on the sensitivity of their dune-erosion predictions to surge level, offshore wave height, and grain diameter, and on the temporal evolution of the dune-erosion volume during a storm. Broadly speaking, all models performed about the same and sometimes produced quite unrealistic results. Because XBeach is the only model that can be run in area mode and can thus handle alongshore variability in beach and dune characteristics, Walstra et al. (2008) proposed to further develop XBeach into the process-based dune-erosion method that has to replace DUROS+ in complicated coastal settings. This further development requires 1) more advanced process descriptions of, for example, sand transport; 2) improvements to various numerical issues, such as the possibility to use curvi-linear grids; 3) extensive validation with existing and new field and laboratory data sets; and 4) the embedding of the predictions in a probabilistic setting. The next two sections of this paper focus on recent laboratory and field measurements that were motivated by the effect of the very gentle beach slopes typical of the Wadden islands on the water motion, sand transport and beach profile evolution, including dune erosion.

Fig. 6. Beach-plain at the western head of Ameland, near the location labeled PTs in Fig. 1. The 4WD car is located on the high-water line. The faint white line just below the horizon is due to wave breaking on the ebb-tidal delta. The beach-plain is covered by up to 1 m high young dunes that are washed away when the beach-plain is flooded during a severe storm.

https://doi.org/10.1017/S0016774600000494 Published online by Cambridge University Press

Laboratory experiments

The small-scale experiments described here were carried out in 2010 in the Scheldegoot at Deltares, Delft, the Netherlands (Hoonhout et al., 2010a, b). The flume has a length of 110 m, a width of 1 m, and a height of 1.2 m. Eleven experiments were carried out, five of which were dune-erosion experiments. The rationale behind these 5 experiments was to create a data set of dune erosion for coastal profiles with a shallow beach-plain and to assess the performance of DUROS+ in hindcasting the measured erosion volume. The initial profile was the same as the reference profile but including an approximately 400 m wide (in prototype) beach-plain (Fig. 3), as found, for example, on Ameland (Fig. 6). The experimental conditions are shown in Table 1, including the code to identify each experiment. During experiment A1a, the wave and water level conditions varied as proposed by Vellinga (1983, 1986), see also Fig. 4b. The purpose of A1a and A2a was to validate the assumption that the erosion volume due to time-varying conditions (A1a) can be approximated well by using the time-invariant conditions (A2a) for a period of 5 hours at prototype scale, also when the profile deviates from the reference profile. B1a and B2a are variations on A2a, differing in wave height (B1a) and period (B2a). Experiment C1a equals A2a but is based on the reference profile without the beach-plain. All experiments lasted for 5 hours, corresponding to 32 hours in prototype. During each experiment the cross-shore profile was measured 6 times. Also, water levels and flow velocities were measured to obtain data to guide the further development and testing of a process-based dune erosion model. The grain size in model was about 110 µm.

Figure 7 compares the cumulative erosion volume for tests A1a and A2a. Similar to the results in Fig. 4 with the reference profile, most of the erosion takes places when the water level is highest. The total amount of erosion with the time-varying conditions equals the erosion with the time-invariant conditions after about 4 to 5 hours in prototype, similar to what was observed by Vellinga (1983, 1986) for the reference profile (Fig. 4). The presence of the beach-plain reduced the erosion volume above surge level by 85%, from about 312 m^3/m in C1a to 47 m^3/m in A2a. Both the about 20% increase in H_{0s} (A2a versus B1a) and 35% increase in T_p (A2a versus B2a) caused the dune erosion volume to become larger, by about 35% and 5%,

Table 1. Experimental conditions (after Hoonhout et al., 2010b).

Experiment	Prototype		Model		
	H_{0s} (m)	T_p (s)	H_{0s} (m)	T_p (s)	h* (m)
A1a	varying	varying	varying	varying	varying
A2a	9.0	14.2	0.225	2.25	0.70
B1a	10.7	14.2	0.267	2.25	0.70
B2a	9.0	18.9	0.225	3.00	0.70
C1a	9.0	14.2	0.225	2.25	0.70

* h is the water depth at the seaward end of the cross-shore laboratory profile.

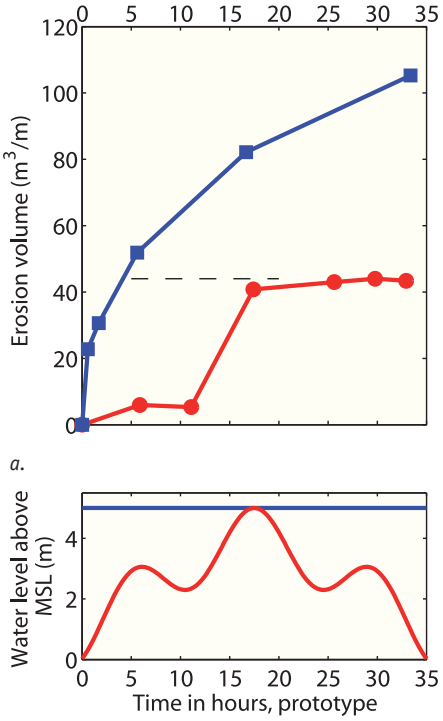

a.

b.

Fig. 7. a. Temporal evolution of the erosion volume above storm surge level (in prototype) during tests A1a (in red) and A2a (in blue). Panel (b) shows the corresponding water level series. The dashed black line in (a) indicates that the erosion volume in the test with time-varying water levels is reached after about 5 hours with constant maximum water level (after Hoonhout et al., 2010a).

respectively. The dependence of the erosion volume on T_p is less than observed previously for the reference profile; the reason for this is not known. Figure 8 shows that the DUROS+ predictions are slightly larger than the observed erosion volumes for all tests. From a coastal-management point of view, this is advantageous, as it is better to over- rather than to underestimate the amount of dune erosion.

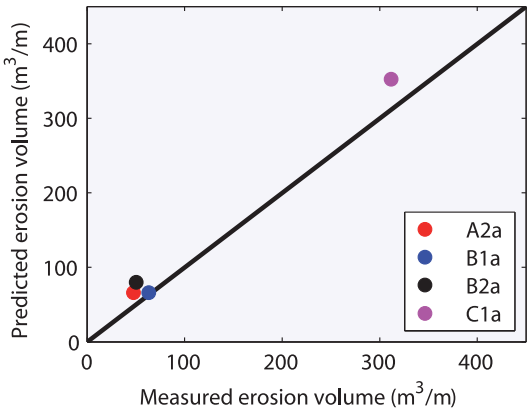

Fig. 8. DUROS+ predicted versus measured erosion volume (in prototype) above surge level for experiments A2a, B1a, B2a and C1a. The diagonal line is the line of equality. (after Hoonhout et al., 2010a).

https://doi.org/10.1017/S0016774600000494 Published online by Cambridge University Press

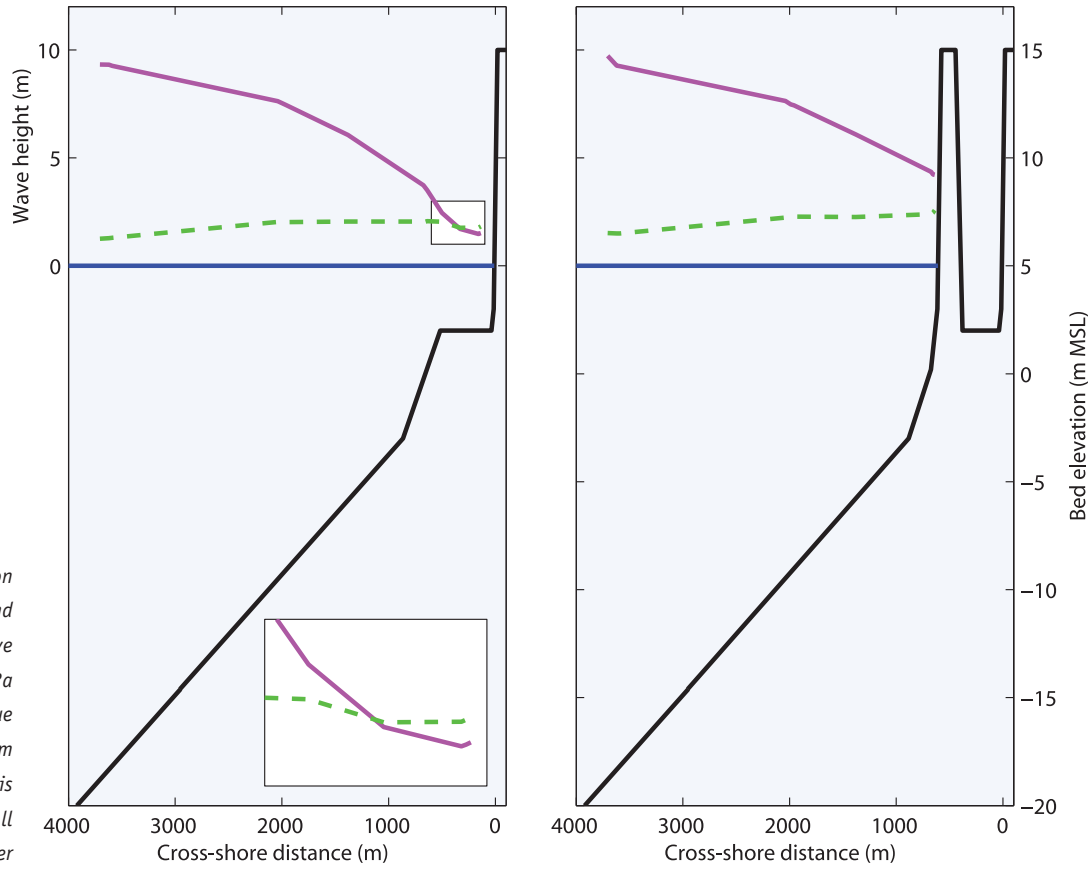

Fig. 9. Cross-shore evolution of the short (magenta) and infragravity (green) wave height for experiments A2a (a) and C1a (b). The blue line is the water level (5 m +MSL) and the black line is the bed-elevation profile. All values are prototype. (after Hoonhout et al., 2010a).

Figure 9 illustrates the cross-shore evolution of the prototype wave height for both the short (i.e., 'storm') and infragravity waves. As expected, the beach-plain causes a more marked decrease in the short-wave height. This decrease is so substantial that the wave motion on the beach plain is dominated by infragravity waves (Fig. 9a), consistent with field observations on very gently sloping beaches by, for example, Ruessink et al. (1998a) and Ruggiero et al. (2004). Interestingly, also the infragravity-wave height decreases across the beach-plain. This is consistent with earlier field observations on very gently sloping profiles (e.g., Ruessink, 1998). Why infragravity waves lose part of their energy is neither obvious from the present laboratory nor from the previous field data. We return to this point in the next section. Because of a lack of detailed flow and sand-concentration measurements, it is difficult to reason why the presence of the beach-plain reduces the dune erosion volume so profoundly. Conceptually, the reduced short-wave height just seaward of the dune face will cause less intense slumping and retreat of the dune face. Furthermore, the reduced short-wave height will cause less sand stirring seaward of the retreating dune face and in a less pronounced undertow, hence in a much reduced offshore transport.

Field studies

Extensive field campaigns to measure the water motion, sand transport and evolving bathymetry of a beach have been carried out since the mid 1970s. In the Netherlands, most campaigns were carried out at the Holland coast, most notably at the beaches of Groote Keeten and Egmond aan Zee (e.g., Ruessink et al., 2001; Price & Ruessink, 2008). Field campaigns on the beaches of the Wadden islands have been scarcer. As part of the EU-funded NOURTEC project, Ruessink et al. (1998b) investigated the role of storm waves, infragravity waves and mean flows to the cross-shore transport in 3 to 9 m water depth, well seaward of the intertidal beach and the dunes, at Terschelling. Van der Vegt et al. (2009) examined the hydrodynamical processes responsible for the migration of a small channel in a secondary tidal inlet system on the island of Texel. In the remainder of this section, we focus on the 2010 Ameland campaign. This campaign was set-up specially to better understand the mutual interaction between water motion (turbulence, waves, mean flows), sand suspension and transport, and morphological change of a gently sloping beach during high-energy wave conditions in shallow (less than 2 m depth) water. The collected data are expected to be useful to guide the development and to test the process-based model that will replace DUROS+ for complicated coastal settings.

https://doi.org/10.1017/S0016774600000494 Published online by Cambridge University Press

The 2010 Ameland field campaign

The field campaign was conducted from September 22, 2010, to November 1, 2010, at the northernmost tip of the western head of Ameland, the Netherlands (Fig. 1, label 'PTs'). The scientific focus was on quantifying the importance of breaking-induced, surface-generated turbulence to sand suspension and on the cross-shore structure of infragravity waves. As mentioned in the Introduction section of this article, surface-generated turbulence is likely the major source for sand suspension under storm conditions, while infragravity waves are one of the mechanisms expected to transport the suspended sand in the seaward direction and hence to contribute to beach and dune erosion. The beach is very low-sloping (~1:80), borders an approximately 400-m wide beach-plain (Fig. 6), is protected from the full force of North Sea waves by a spatially extensive, shallow ebb-tidal delta, and is located at a strongly curved coast (Fig. 1).

During the campaign, 14 pressure transducers (PTs) were deployed with an approximately 10-20 m spacing in a cross-shore transect from just below the spring low-tide level to the high-tide level expected for a typical autumn storm coinciding with spring tide (Fig. 10a). The instrument positions are labeled P1 to P14 in the onshore direction. At three of these positions (P7, P9 and P11), electromagnetic flow meters, and vertical stacks of optical backscatter sensors were also deployed to measure the near-bed horizontal flow and sand concentrations (Fig. 10b). At P5, a rig (Fig. 10c) was deployed to study the vertical structure of turbulence, oscillatory flow, cross-shore and alongshore mean flow, and sand concentration beneath breaking waves, see also Ruessink (2010). Sensors used here include three single-point, downward-oriented, 5-MHz Sontek acoustic Doppler velocimeter ocean (ADVO) probes to measure turbulence, and a stack of 5 optical backscatter sensors to measure sand concentrations. At the remaining 10 positions, stand-alone PTs (Fig. 10d) were deployed. At all locations, measurements were performed continuously with a sampling frequency of 4 or 5 Hz when the instruments were submerged. The three ADVOs sampled at 10 Hz in bursts of approximately 29 minutes each half hour. The median grain size was about 200 µm.

Figure 11 shows the wave and water level conditions during the field campaign. The offshore wave data, measured by a directional buoy in about 22 m depth seaward of the ebb-tidal delta (labeled B12 in Fig. 1) and by a non-directional buoy in about 4 m depth landward of the delta (labeled B22 in Fig. 1), comprise 10-minute values of the spectral significant wave height H_{0s}, mean period T and (for buoy B12 only) angle of wave incidence θ in the 30-500 mHz frequency band. The experiment average H_{0s} and T seaward of the delta were approximately

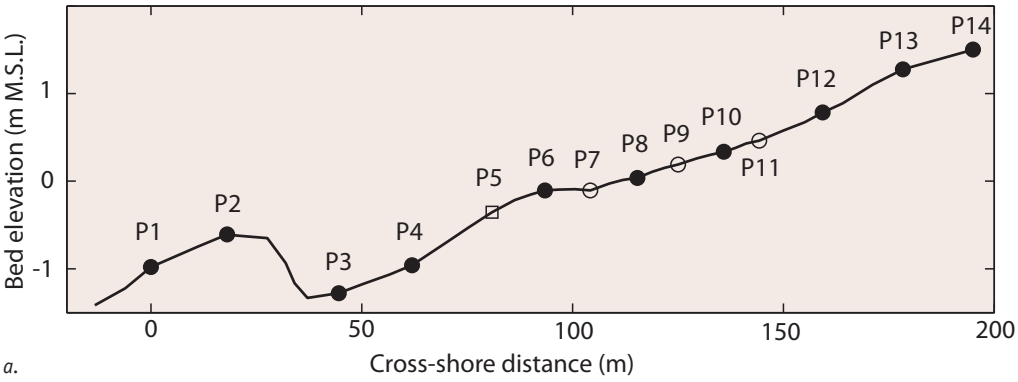

a.

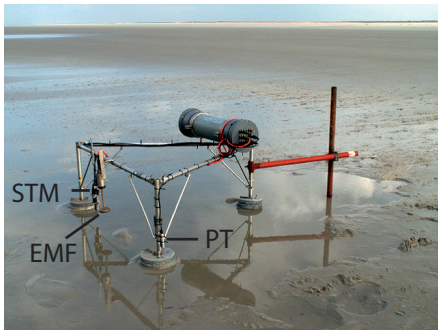

b.

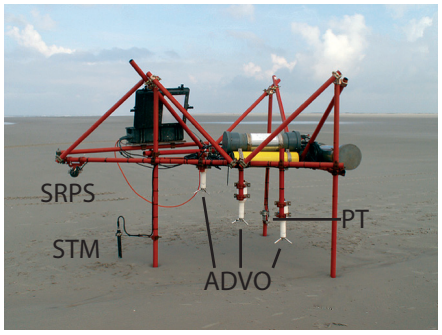

c.

d.

Fig. 10. a. Cross-shore profile measured at the start of the Ameland 2010 field campaign. The open circles are the locations of the instrument rigs in (b). Rig (c) was located at P5 (square). Pressure transducers as shown in (d) were deployed at the other locations (filled circles). The instrument abbreviations are PT = pressure transducer, ADVO = acoustical Doppler velocimeter Ocean, EMF = electromagnetic flow meter, STM = Seapoint turbidity meter (= optical backscatter sensor), and SRPS = sand ripple profiling sonar. An approximately 500-m wide beach-plain (Fig. 6) separates P14 from the dunefoot.

https://doi.org/10.1017/S0016774600000494 Published online by Cambridge University Press

1.45 m and 4.7 s, respectively. The wave height peaked during a storm on yearday 297 (October 24, 2010) with a value just below 6 m (Fig. 11a). Figure 11a clearly demonstrates the effect of the delta on wave characteristics, as the wave height shoreward of the delta is tide-modulated (compare Fig. 11a to Fig. 11d) and never reaches above 1.9 m. The water levels are 10-minute values for the tidal station Terschelling Noordzee (labeled TN in Fig. 1), see Fig. 11d. Surge levels (Fig. 11e) were estimated as the difference between measured and predicted tide, and reached values up to +0.65 m during the most energetic events and –0.7 m during mild conditions. In the following we present snapshots of the turbulence and infragravity-wave results. Details of data processing are given in Pieterse (2011) and De Bakker (2011), and are not reiterated here.

Turbulence beneath breaking waves

Turbulence levels were quantified by means of the Froude-scaled turbulent kinetic energy $\sqrt{k/gh}$. Here, the turbulent kinetic energy k is defined as $k = 0.5\left(\langle u'^2\rangle + \langle v'^2\rangle + \langle w'^2\rangle\right)$, g is gravitational acceleration, h is water depth, and the angle brackets denote a burst-average. The instantaneous (i.e. 10 Hz) cross-shore, alongshore, and vertical turbulence fluctuations (u', v' and w', respectively) were estimated for each ADV0 using the two-sensor separation technique of Feddersen et al. (2007). Turbulence estimates that did not pass the criteria given in Feddersen (2010) were removed from the data set. Figure 12a shows $\sqrt{k/gh}$ versus the local relative wave height, defined as the ratio of the significant wave height H_s to the water depth. This ratio can be seen as a measure of breaking intensity, with waves starting to break at $H_s/h \approx 0.3$ (Ruessink et al., 1998b).

Under non-breaking waves ($H_s/h < 0.3$), turbulence levels are low ($\sqrt{k/gh} < 0.02$) and do not depend on the relative sensor height above the bed, ξ/h (Fig. 12b). We do not see an increase in turbulence levels very close to the bed, indicative of turbulence generated near the bed because of strong shear in oscillatory and mean flows (e.g., Nadaoka and Kondoh, 1982). Possibly, the measurements did not extend close enough to the bed for $H_s/h < 0.3$ to witness this near-bed increase in $\sqrt{k/gh}$. With an increase in H_s/h, turbulence levels intensify in the entire water column, and especially so higher up in the column. For $H_s/h = 0.3$-0.5 the increase in $\sqrt{k/gh}$ is most marked for $\xi/h > \approx 0.3$ (Fig. 12c), while for $Hs/h > 0.5$ the increase is notable in the entire water column (Fig. 12d). Thus, Figures 12c-d signify that for $H_s/h > \sim 0.3$ turbulence is generated predominantly at the sea surface due to wave breaking and that, as wave breaking intensifies, this turbulence penetrates deeper into the water column towards the bed. The effect hereof on sand suspension and transport is currently being investigated; preliminary results can be found in Pieterse (2011) and will be presented in more detail elsewhere.

Infragravity waves

The significant height of the infragravity waves on the intertidal beach varied between approximately 0.02 and 0.67 m, with the variations closely linked to the offshore short-wave significant wave height (H_{s0} at buoy B12). At P1, for example, the correlation coefficient amounted to 0.85. The constant of proportionality between the significant infragravity-wave height at P1 and H_{s0} at buoy B12 was about 0.11, and increased to 0.14 at P12.

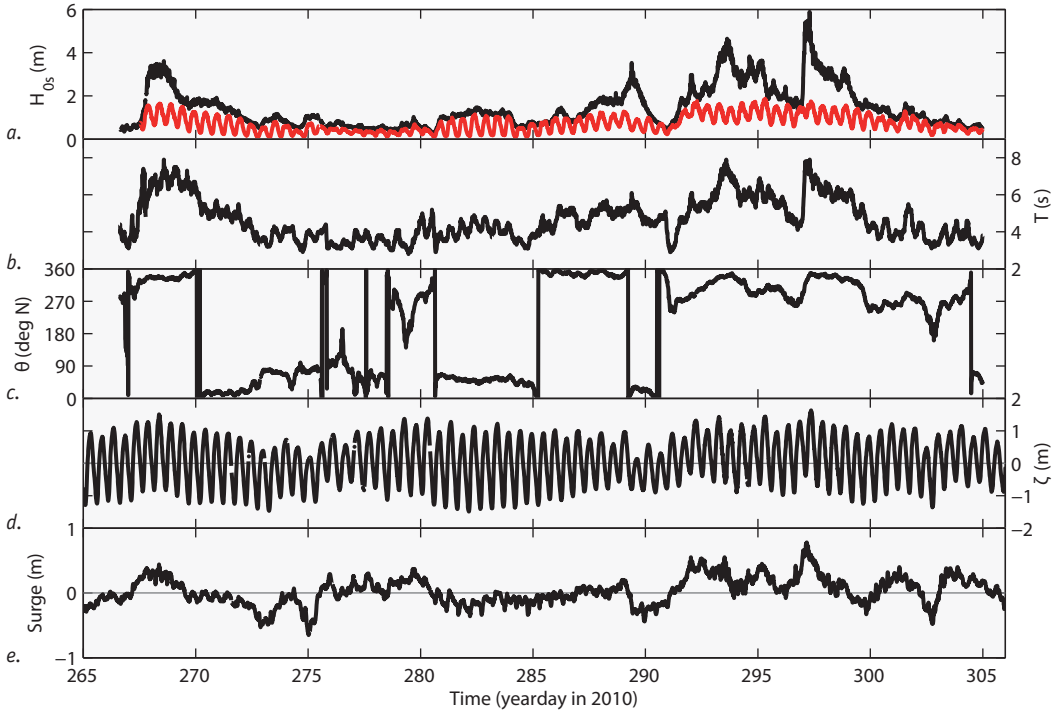

Fig. 11. a. Offshore significant wave height H_{s0} (black line, buoy B12; red line, buoy B22); b. mean period T; c. angle of incidence θ; d. water level ζ with respect to MSL; and e. surge level versus time. Unless otherwise indicated, the wave data were measured at B12 and the water level data at TN, see Fig. 1 for location. The shore-normal direction of the instrument array is about 0° N.

https://doi.org/10.1017/S0016774600000494 Published online by Cambridge University Press

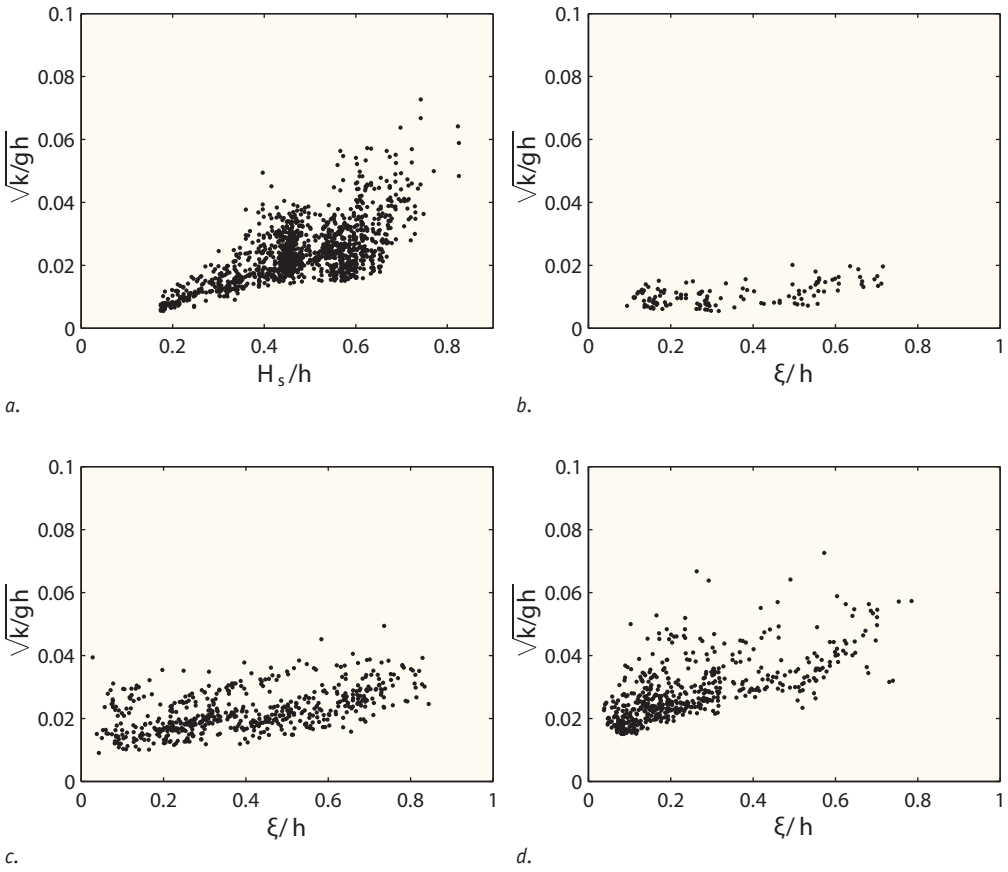

Fig. 12. Froude-scaled turbulent kinetic energy $\sqrt{k/gh}$; a. versus the relative wave height H_s/h (all observations), and versus the normalised sensor height above the bed ξ/h; with b. $H_s/h < 0.3$; c. $H_s/h = 0.3$-0.5; and d. $H_s/h > 0.5$ at P5. $\xi/h = 0$ is the sea bed, $\xi/h \approx 0.7$ is the approximate wave trough level.

Figure 13 examines the measured cross-shore structure of infragravity waves at a representative high tide (here, during the storm on September 25, 2010). The left column in Fig. 13 is representative of the highest infragravity-wave periods (>60 s) and shows the classical picture of a standing infragravity wave: the pressure fluctuations have clear amplitude E maxima (at the shore, x ≈ 160 m, and on the bar, x ≈ 25 m; Fig. 13a) and minima (x ≈ 130 m); a phase φ jump of ±180 degrees is located at the minimum (Fig. 13b); and, the reflection coefficients R^2 are well above 0.5 (Fig. 13c). This standard picture starts to change with a decrease in period. For the 30-60 s range the amplitude still has some amplitude fluctuations (Fig. 13d), but

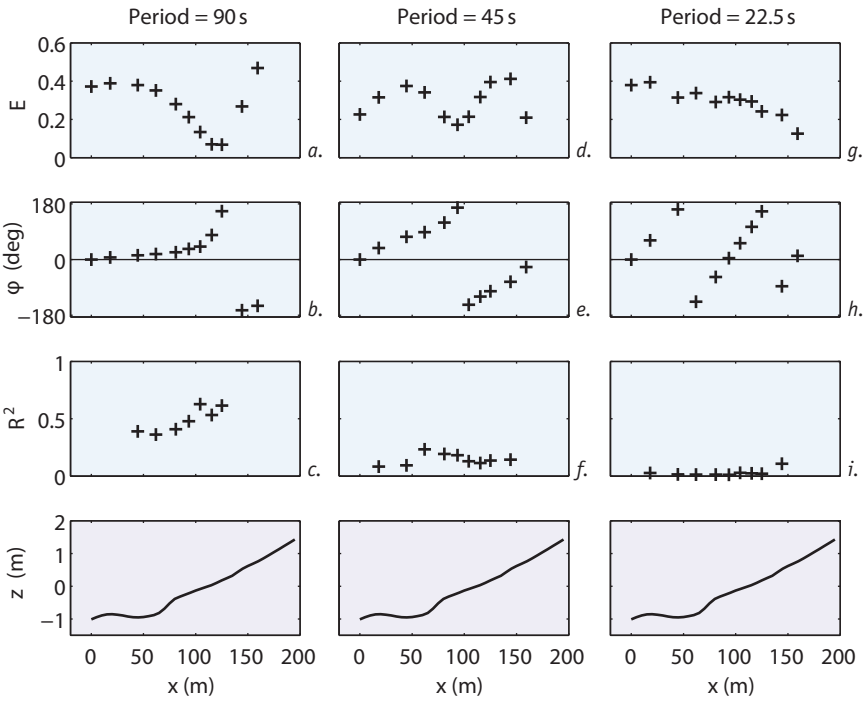

Fig. 13. (from top to bottom) Non-dimensional amplitude E, phase φ, reflection coefficient R^2 and bed elevation z versus cross-shore distance x. Left panels: period = 90 s; middle panels = 45 s; right panels = 22.5 s. The amplitude E and phase φ were extracted from an eigenfunction analysis of the cross-spectral matrix for each period, see Henderson et al. (2000) for details. The reflection coefficients R^2 were obtained using the Van Dongeren et al. (2007) methodology to split the total infragravity motion into shoreward and seaward propagating components. The bed elevation is with respect to Mean Sea Level, MSL, and cross-shore distance is with respect to P1. The results in (a-i) were based on a 2-hr record of near-bed pressure at each measurement location. The offshore significant wave height (in 22-m depth) amounted to 3.5 m and the tide level was about 1 m above MSL (high tide). Short waves broke over the entire measurement profile.

https://doi.org/10.1017/S0016774600000494 Published online by Cambridge University Press

the phase jump has been replaced by an increase in phase to the shore (Fig. 13e) and the reflection coefficients have dropped to about 0.2 (Fig. 13f). The 30-60 s period range is thus characterised by a mixture of shoreward-progressive and standing waves. The standing pattern completely disappears for lower infragravity-wave periods: the amplitude decreases to the shore monotonically (Fig. 13g); the phase evolution is as expected for an onshore progressive wave (Fig. 13h); and the reflection coefficients are less than 0.05 (Fig. 13i). The bulk (i.e. integrated over the entire infragravity-period range) reflection coefficient at the shallowest position (x = 125 m) is about 0.35 only. This implies that some 65% of the shoreward infragravity energy flux must dissipate shoreward of x = 125 m, in water depths less than 0.5-1 m, including the swash zone (i.e. the region where waves run up and down the beach). This represents a remarkably localised source of dissipation, considering the short stretch in which it occurs (the distance between x = 125 m and the shoreline is some 50 m). It also represents a major difference with findings on steeper beaches where reflection coefficients in this depth range are about 1 (e.g., Sheremet et al., 2002; Thomson et al., 2006) and inshore dissipation is thus negligible. Also, most infragravity-wave models are non-dissipative. On a 1:35 laboratory beach, Van Dongeren et al. (2007) also found localised, inshore infragravity-wave dissipation. They noted how shoreward propagating infragravity waves changed shape and postulated that this was indicative of breaking.

Figure 14 tests whether the results in Fig. 13 for the lower infragravity-wave periods (say, <60 s) are consistent with the hypothesis of infragravity-wave breaking. In this figure, the reflection coefficients at P11 (the most shallow location submerged during virtually all high tides) estimated for all 75 high tides during the Ameland campaign are plotted versus a parameter that delineates the steep-slope (no dissipation, full reflection from the shoreline) from the mild-slope (breaking-induced dissipation, incomplete reflection) regime. This parameter, proposed by Van Dongeren et al. (2007), reads as

$$\beta_{max} = \left(\frac{h_x}{\omega}\right)\sqrt{\frac{g}{H}} \qquad (6)$$

where h_x is the beach slope (≈ 1:80), H is the height of the infragravity wave near the shoreline (here, at P11) and $\omega = 2\pi/T$, with T the infragravity-wave period. Figure 14 illustrates that the observed reflection coefficients depend clearly on β_H, with a change from the steep-slope to the mild-slope regime at $\beta_H \approx 2$. Indeed, the longer periods (T = 90 s) are in the steep-slope regime ($\beta_H > \approx 2$), while most of the shorter periods (T = 22.5 s and 45 s) are in the mild-slope regime ($\beta_H < \approx 2$). On the whole, Figure 14 supports the hypothesis that infragravity-wave breaking is the major source for infragravity-wave dissipation and may explain why the infragravity-wave height reduces across the laboratory beach-plain (Fig. 9). Further work is required to more extensively prove the relevance of breaking to infragravity-wave dynamics

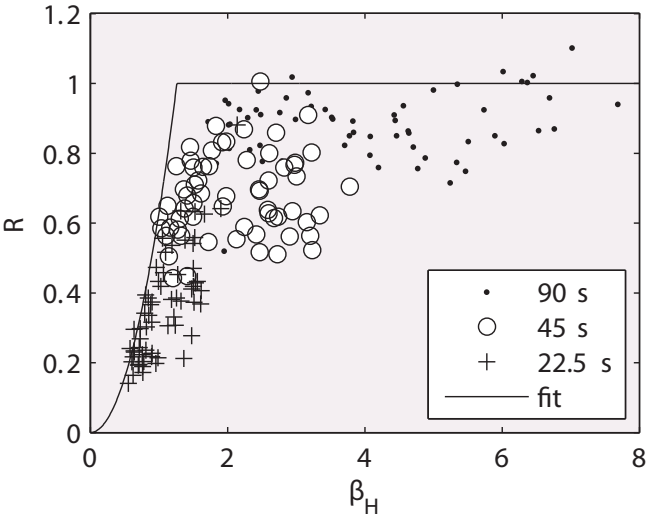

Fig. 14. Reflection coefficient R at 3 infragravity-wave periods (90 s, 45 s and 22.5 s) versus the breaker parameter β_H at P11. The fit is a theoretical prediction ($R = 0.2\pi\beta_H^2$) given in Van Dongeren et al. (2007), in which the steep-slope regime (i.e., no dissipation, hence R = 1) starts at $\beta_H = 1.25$. In the Ameland data, the steep-slope regime appears to start around $\beta_H = 2$.

on gently sloping beaches typical of the Wadden islands and to explore if and how infragravity-wave dissipation alters the erosion magnitude and rate of dunes bordered by gently sloping beaches or beach-plains compared to those bordered by steeper beaches.

Concluding remarks

The accurate assessment of dunes to withstand a severe storm is of utmost importance to low-lying, densely populated coastal regions such as the Netherlands. Within Dutch coastal management, an equilibrium-based dune-erosion model embedded within a probabilistic setting has been used since the 1980s to estimate whether a dune is sufficiently wide to not breach during a storm with a 1 in 10,000 frequency of occurrence. The presently used equilibrium model, DUROS+, is the result of a large number of laboratory experiments. It predicts the equilibrium post-storm beach and dune profile as a function of the offshore significant wave height, period and water level, of the sand fall velocity and of the initial profile. The laboratory experiments all used a highly schematised cross-shore profile of the rather alongshore uniform Holland coast – the reference profile – as initial profile. The presence of ebb-tidal deltas, tidal channels, strong coastal curvature, narrow and low dune ridges, and extensive beach-plains compromise the validity of DUROS+ estimates for large parts of the Wadden islands and have led to the suggestion that a process-based and spatially extensive model should be set-up to replace DUROS+ as the dune-erosion model in complicated coastal settings.

A process-based model aims to predict the interaction between the water motion (waves, wave-induced flows), sand suspension and transport, and the bathymetry in a time-stepping

https://doi.org/10.1017/S0016774600000494 Published online by Cambridge University Press

manner. Results like those presented in Figs 9, 12, 13 and 14 highlight just some of the challenges we are facing to develop and test such a model. Firstly, the sand transport equations in many coastal-evolution models are engineering type models that are based on laboratory experiments with non-breaking waves (e.g., Ribberink, 1998; Silva et al., 2006) and assume that bed-generated turbulence is the dominant source of turbulence to stir sediment. Attempts to include the effect of surface-generated turbulence in sand transport modelling have been made by, for example, Deigaard et al. (1986), Roelvink and Stive (1989) and Mocke (2001). These models remain largely untested because of a lack of simultaneously collected data of the vertical structure of turbulence and sand suspension under field conditions. The Ameland data, as well as the ECORS-TrucVert'08 field data (Ruessink, 2010; Sénéchal et al., 2011), offer unique possibilities to test and improve these models, such that coastal-evolution models can make more realistic predictions of beach and dune erosion during storms. Secondly, the decline in infragravity-wave height on the laboratory beach-plain and the limited reflection of infragravity waves with periods <60 s from the 1 : 80 natural beach challenge our textbook view that infragravity waves are cross-shore standing waves that increase in amplitude towards the coast. Infragravity dissipation, most likely due to breaking, is not considered by most infragravity-wave models, yet infragravity waves are likely to be one of the main mechanisms to transport the suspended sediment seaward. Neither the laboratory nor the field measurements have provided insight in the cross-shore and vertical structure of another transporting mechanism under breaking waves, the undertow.

The improved description of the water motion and sand transport under breaking waves in front of an eroding dune is only one of the many aspects to be considered in the design of a process-based dune-erosion model. The complicated coastal setting demands the use of a spatially extensive model, incorporating wave transformation, (tidal) flow, and wave-current interaction over ebb-tidal deltas, in channels, and along the curved heads of the Wadden islands. Remote sensing of the sea surface is likely to be the key technique to obtain wave and flow information over vast areas, as demonstrated by Gautier and Van der Westhuyzen (2010) and Swinkels (2010) for the tidal delta and inlet between Terschelling and Ameland using an X-band radar system mounted on the Ameland lighthouse. The remotely sensed flow patterns suggested a different horizontal structure of the tidal flow in the inlet than produced by a hydrodynamic model with default setting. Based on a number of model sensitivity tests, Swinkels (2010) obtained better model-data agreement when the model was run with a spatially varying bed roughness. We believe that in-situ and remote-sensing field observations, laboratory experiments and numerical models are the pillars of Earth Scientific research in the Wadden Sea area to construct a meaningful dune-erosion tool.

Acknowledgements

The work presented here received funding from a variety of projects. BGR and RCW acknowledge funding by Utrecht University's focus area 'Earth and Sustainability', subtheme 'Earth and Climate'. FG was funded by the Netherlands Organization for Scientific Research under project 825.10.035 (Rubicon/Marie Curie Cofund Action). The work presented here has benefitted greatly from extensive discussions in the framework of the Sterkte en Belastingen Waterkering (SBW) project, commissioned by Rijkswaterstaat Waterdienst and carried out by Deltares.

References

Boers, M., Diermanse, F. & Van Dongeren, A., 2011. Flood hazard maps in coastal areas. *In:* Proceedings of CoastGIS 2011, Vol. 4: 67-74.

Carter, R.W.G. & Stone, G.W., 1989. Mechanisms associated with the erosion of sand dune cliffs, Magilligan, Northern Island. Earth Surface Processes and Landforms 14: 1-10.

Coeveld, E.M., Den Heijer, C., Van de Graaff, J., De Vroeg, J.H. & Steetzel, H.J., 2005. The effect of wave period on dune erosion. *In:* Proceedings Coastal Dynamics'95. ASCE, New York, 11 pp.

De Bakker, A.T.M., 2011. Infragravity waves: propagation, dissipation and sediment transport in the inner surf zone of a low sloping beach. MSc thesis, Utrecht University, 84 pp.

Deigaard, R., Fredsøe, J. & Brøker-Hedegaard, I., 1986. Suspended sediment in the surf zone. Journal of Waterways, Port, Coastal and Ocean Engineering, 112: 115-127.

Deltares, 2007. Dune erosion. Product 3: Probabilistic dune erosion prediction method. Report H4357/A1414, 86 pp.

Diermanse, F., Walstra, D.J., Smale, A., Van Geer, P. & Huisman, B., 2011. Detailtoets voor duinafslag. Afleiden van de rekenregel ten behoeve van WTI 2011. Deltares Report 1202124-003-HYE-0001, 126 pp. (In Dutch)

ENW, 2006. Technisch Rapport Duinafslag. Beoordeling van de veiligheid van duinen als waterkering ten behoeve van Voorschrift Toetsing op Veiligheid 2006. Lecturis, Eindhoven, 59 pp. (In Dutch)

Feddersen, F., Trowbridge, J.H. & Williams III, A.J., 2007. Vertical structure of dissipation in the nearshore. Journal of Physical Oceanography 37: 1764-1777.

Feddersen, F., 2010. Quality controlling surfzone acoustic doppler velocimeter observations to estimate the turbulent dissipation rate. Journal of Atmospheric and Oceanic Technology 27: 2039-2055.

Gautier, C. & Van der Westhuyzen, A., 2010. Wave propagation under the influence of currents. Deltares Report 1202119-001-HYE-0002, 129 pp.

Henderson, S.M., Elgar, S. & Bowen, A.J., 2000. Observations of surfbeat propagation and energetics. *In:* Proceedings 27th International Conference on Coastal Engineering. ASCE, New York: 1412-1421.

Hoonhout, B., Van Geer, P., McCall, R. & Boers, M., 2010a. Duinafslag en -overslag bij brede stranden. Deel A: toepasbaarheid van DUROS bij kustprofielen met een breed strand. Deltares Report 1202124-007-HYE-0002, 20 pp. (In Dutch)

Hoonhout, B., Van Geer, P. & McCall, R., 2010b. Dune erosion and overwash at wide beaches. Part B: measurement results of experiments in the Scheldt Flume. Deltares Report 1202124-007-HYE-0001, 169 pp.

Huisman, B.J.A., De Grave, P., Diermanse, F.L.M., Walstra, D.J.R. & Van Thiel de Vries, J.S.M., 2010. Ontwikkeling detailtoets duinen 2011 (D++). Deltares Report 1202124-003-HYE-0004, 125 pp. (In Dutch)

Larson, M. & Kraus, N.C., 1989. SBEACH: numerical model for simulating storm-induced beach change. Report 1. Empirical foundation and model development. US Army Corps of Engineers Technical Report CERC-89-9, US Army Engineer Waterways Experiment Station, Vicksburg, MS.

Larson, M., Erikson, L. & Hanson, H., 2004. An analytical model to predict dune erosion due to wave impact. Coastal Engineering 51: 675-696.

McCall, R.T., Van Thiel de Vries, J.S.M., Plant, N.G., Van Dongeren, A.R., Roelvink, J.A., Thompson, D.M. & Reniers, A.J.H.M., 2010. Two-dimensional time dependent hurricane overwash and erosion modeling at Santa Rosa Island. Coastal Engineering 57: 668-683.

McNinch, J.E., 2004. Geologic control in the nearshore: shore-oblique sandbars and shoreline erosional hotspots, Mid-Atlantic Bight, USA. Marine Geology 211: 121-141.

Mocke, G.P., 2011. Structure and modeling of surf zone turbulence due to wave breaking. Journal of Geophysical Research, 106: 17,039-17,057.

Nadaoka, K. &. Kondoh, T., 1982. Laboratory measurements of velocity field structure in the surf zone by LDV. Coastal Engineering in Japan 25:125-145.

Nadaoka, K., Ueno, S. & Igarashi, T.,1988. Sediment suspension due to large scale eddies in the surf zone. *In:* Proceedings of the 21st Conference on Coastal Engineering. ASCE, New York: 1646-1660.

Nishi, R. & Kraus, N.C., 1996. Mechanism and calculation of sand dune erosion by storms. *In:* Proceedings of the 25th Conference on Coastal Engineering. ASCE, New York: 3034-3047.

Overton, M.F., Pratikto, W.A., Lu, J.C. & Fisher, J.S., 1994. Laboratory investigation of dune erosion as a function of sand grain size and dune density. Coastal Engineering 23: 151-165.

Pieterse, A., 2011. Downward spreading of turbulence beneath breaking waves and its influence on sediment suspension. MSc thesis, Utrecht University, the Netherlands, 98 pp.

Price, T.D. & Ruessink, B.G., 2008. Morphodynamic zone variability on a microtidal barred beach. Marine Geology 251: 98-109

Ribberink, J.S., 1998. Bed-load transport for steady flows and unsteady oscillatory flows. Coastal Engineering 34: 59-62.

Roelvink, J.A. & Stive, M.J.F., 1989. Bar-generating cross-shore flow mechanisms on a beach. Journal of Geophysical Research, 94: 4785-5800.

Roelvink, D., Reniers, A., Van Dongeren, A., Van Thiel de Vries, J., McCall, R. & Lescinski, J., 2009. Modeling storm impacts on beaches, dunes and barrier islands. Coastal Engineering 56: 1133-1152.

Ruessink, B.G., 1998. The temporal and spatial variability of infragravity waves in a barred nearshore zone. Continental Shelf Research 18: 585-605.

Ruessink, B.G., Kleinhans, M.G. & Van den Beukel, P.G.L., 1998a. Observations of swash under highly dissipative conditions. Journal of Geophysical Research 103: 3111-3118.

Ruessink, B.G., Houwman K.T. & Hoekstra, P., 1998b. The systematic contribution of transporting mechanisms to the cross-shore sediment transport in water depths of 3 to 9 m. Marine Geology 152: 295-324.

Ruessink, B.G., Miles, J.R., Feddersen, F., Guza,R.T. & Elgar, S., 2001. Modeling the alongshore current on barred beaches. Journal of Geophysical Research 106: 22451-22464.

Ruessink, B.G. & Jeuken, M.C.J.L., 2002. Dunefoot dynamics along the Dutch coast. Earth surface processes and landforms 27: 1043-1056.

Ruessink, B.G., 2010. Observations of turbulence within a natural surf zone. Journal of Physical Oceanography 40: 2696-2712.

Ruggiero, P., Holman, R.A. & Beach, R.A., 2004. Wave runup on a high-energy dissipative beach, Journal of Geophysical Research 109: C06025, doi:10.1029/2003JC002160.

Russell, P., 1993. Mechanisms for beach erosion during storms. Continental Shelf Research 13: 1243-1265.

Schupp, C.A., McNinch, J.E. & List, J.H., 2006. Nearshore shore-oblique bars, gravel outcrops, and their correlation to shoreline change. Marine Geology 233: 63-79.

Sénéchal, N., Abadie, S., Gallagher, E., MacMahan, J., Masselink, G., Michallet, H., Reniers, A., Ruessink, G. Russell, P., Sous, D., Turner, I., Ardhuin, F., Bonneton, P., Bajun, S., Capo, S., Certain, R., Pedreros, R. & Garlan, T., 2011. The ECORS-Truc Vert 2008 nearshore field experiment: presentation of a three-dimensional morphologic system in a macrotidal environment during consecutive extreme storm conditions. Ocean Dynamics, 61: 2073-2098.

Sheremet, A., Guza, R.T. Elgar, S. & Herbers, T.H.C., (2002), Observations of nearshore infragravity waves: 1. Seaward and shoreward propagating components, Journal of Geophysical Research, 107: 3095, doi:10.1029/2001JC000970.

Short, A.D., 1992. Beach systems of the central Netherlands coast: processes, morphology and structural impacts in a storm driven multi-bar system. Marine Geology 107: 103-132.

Silva, P.A., Temperville, A. & Santos, F.S., 2006. Sand transport under combined current and wave conditions: a semi-unsteady, practical model. Coastal Engineering 53: 897-913.

Steetzel, H.J., 1993. Cross-shore transport during storm surges. Ph.D. thesis, Delft University of Technology, Delft, the Netherlands.

Steetzel, H.J., 2002. Effect van zwaardere golfcondities op duinenkust. Verkenning effect grotere golfhoogte en langere golfperiode op mate duinafslag en veiligheid duinenkust. Alkyon Report A963. (In Dutch)

Swinkels, C.M., 2010. Storm hindcast January 2010. Analysis of the application of radar current data for hindcast purposes. Deltares Report 1202119-001-HYE-0003, 36 pp.

Thomson, J., Elgar, S., Raubenheimer, B., Herbers, T.H.C. & Guza, R.T., 2006. Tidal modulation of infragravity waves via nonlinear energy losses in the surf-zone, Geophysical Research Letters, 33: L05601, doi:10.1029/2005GL025514.

TAW, 1995. Basisrapport Zandige Kust behorende bij de leidraad Zandige Kust. Technische Adviescommissie voor de Waterkeringen, Delft, 507 pp. (In Dutch)

Van Alphen, J.S.L.J. & Damoiseaux, M.A., 1987. A morphological map of the Dutch shoreface and adjacent part of the continental shelf (1:250,000). Rijkswaterstaat. Nota NZ-N-87.21/MDLK-R-87.18, 20 pp.

Van de Graaff, J., 1977. Dune erosion during a storm. Coastal Engineering 1: 99-134.

Van de Graaff, J., 1986. Probabilistic design of dunes; an example from the Netherlands. Coastal Engineering 9: 479-500.

Van Dongeren, A.R., Battjes, J.A., Janssen, T.T., Van Noorloos, J., Steenhauer, K., Steenbergen, G. & Reniers, A.J.H.M., 2007. Shoaling and dissipation of low-frequency waves. Journal of Geophysical Research 112: C02011, doi:10.1029/2006JC003701.

Van Gent, M.R.A., Van Thiel de Vries, J.S.M., Coeveld, E.M., De Vroeg J.H., & Van de Graaff, J., 2008. Large-scale dune erosion tests to study the influence of wave periods. Coastal Engineering 55: 1041-1051.

https://doi.org/10.1017/S0016774600000494 Published online by Cambridge University Press

Van Rijn, L.C., Tonnon, P.K., Sánchez-Arcilla, A., Cáceres I. & Grüne, J., 2011. Scaling laws for beach and dune erosion processes. Coastal Engineering 58: 623-636.

Van der Vegt, M., Hoekstra P. & Van Puijvelde, S.P., 2009. Channel migration in a small tidal inlet. *In:* Proceedings of the 6th IAHR symposium on River, Coastal and Estuarine Morphodynamics: 169-176.

Van Thiel de Vries, J.S.M., Van Gent, M.R.A., Walstra, D.J.R. & Reniers, A.J.H.M., 2008. Analysis of dune erosion processes in large-scale flume experiments. Coastal Engineering 55:1028-1040.

Vellinga, P., 1982. Beach and dune erosion during storm surges. Coastal Engineering 6: 361-387.

Vellinga, P., 1983. Predictive computational model for beach and dune erosion during storm surges. *In:* Proceedings Coastal Structures'83. ASCE, New York: 806-819.

Vellinga, P., 1986. Beach and dune erosion during storm surges. Ph.D. thesis, Delft University of Technology, Delft, the Netherlands, 200 pp.

Walstra, D.J.R., Diermanse, F.L.M., Van Geer, P.F.C., Van Thiel de Vries, J.S.M. & Van de Graaff, J., 2008. SBWDuinen2-Ontwikkeltraject. Eerste aanzet tot de ontwikkeling van het 2011 Duintoetsinstrumentarium. Deltares Report H5019.20, 145 pp. (In Dutch)

https://doi.org/10.1017/S0016774600000494 Published online by Cambridge University Press